

Measurement of the spin of the M87 black hole from its observed twisted light

Fabrizio Tamburini,¹[★] Bo Thidé²[†] and Massimo Della Valle^{3,4}[‡]

¹ ZKM, Lorenzstraße 19, Karlsruhe, D-76135 Germany

² Swedish Institute of Space Physics, Ångström Laboratory, Box 537, SE-751 21 Uppsala, Sweden

³ Capodimonte Astronomical Observatory, INAF-Napoli, Salita Moiariello 16, I-80131 Naples, Italy

⁴ European Southern Observatory, Karl-Schwarzschild-Straße 2, D-85748 Garching bei München, Germany.

Accepted XXX. Received YYY; in original form ZZZ

ABSTRACT

We present the first observational evidence that light propagating near a rotating black hole is twisted in phase and carries orbital angular momentum (OAM). This physical observable allows a direct measurement of the rotation of the black hole. We extracted the OAM spectra from the radio intensity data collected by the Event Horizon Telescope from around the black hole M87* by using wavefront reconstruction and phase recovery techniques and from the visibility amplitude and phase maps. This method is robust and complementary to black-hole shadow circularity analyses. It shows that the M87* rotates clockwise with an estimated rotation parameter $a = 0.90 \pm 0.05$ with $\sim 95\%$ confidence level (c.l.) and inclination $i = 17^\circ \pm 2^\circ$, equivalent to a magnetic arrested disk with inclination $i = 163^\circ \pm 2^\circ$. From our analysis we conclude, within a 6σ c.l., that the M87* is rotating.

Key words: black hole physics – gravitational lensing; strong – methods: numerical – methods: data analysis – techniques: image processing

1 INTRODUCTION

Most of the knowledge we have about the Universe comes from observing and interpreting its electromagnetic (EM) radiation. This ranges from visible light caught by the naked eye, to radio and higher photon energy emissions intercepted by advanced telescopes. The information carried by the EM field is encoded, naturally or artificially, into conserved quantities (observables) of the field that are transported from the source to the distant observer where the information can be decoded and recovered. The standard observables are the well-known ten conserved quantities that are concomitant with the ten-dimensional Poincaré group of Noether invariants: the field energy (a single scalar), used, e.g., in radiometry, linear momentum (three components of a vector), used in, e.g., radio communications, angular momentum (three components of a pseudovector), used only partially in radio science and technology, and the center of energy (three components of a vector).

Of these observables, we used, for the first time, the EM angular momentum, which is related to rotation and torque action (Torres & Torner 2011), to measure the rota-

tion of the M87* black hole in a novel way. This observable has not yet been fully exploited in astronomy (Harwit 2003; Thidé et al. 2011; Anzolin et al. 2008). The total angular momentum \mathbf{J} comprises two, in general inseparable, quantities: (1) the spin angular momentum \mathbf{S} (SAM), associated with photon helicity, i.e., the wave polarization, and (2) the orbital angular momentum (OAM) \mathbf{L} , associated with the torque action and electromagnetic vorticity. EM waves carrying OAM are also known as “twisted waves”. This property remains valid down to the single photon level as superpositions of photon eigenstates, each with a well-defined value of SAM and OAM, as described in (Molina-Terriza et al. 2007). Only in the paraxial approximation \mathbf{S} and \mathbf{L} behave as two separate variables. OAM-carrying beams permit the encoding and extraction of more information into and from the electromagnetic radiation emitted by a distant source than any existing method that is based on the intensity of the field only (Torres & Torner 2011; Tamburini et al. 2012). In 2011, a theoretical-numerical study published by Tamburini et al. (2011a), showed that light and radio emitted from an accretion disk (AD) around a massive rotating black hole, are expected to be endowed with specific distributions of OAM due to the model of the AD and general relativity (GR) effects such as Kerr spacetime dragging and mixing and gravitational lensing. An example is the Einstein ring, such as that in the M87 galaxy as observed by the EHT

[★] E-mail: fabrizio.tamburini@gmail.com

[†] E-mail: bt@irfu.se

[‡] E-mail: massimo.dellavalle@inaf.it

team, which surrounds the black hole. The Einstein ring is created by gravitationally lensed beams that, experiencing an anamorphic transformation (Beckwith & Done 2005), is also accompanied by a polarization rotation (Su & Mallett 1980) due to the gravitational Faraday effect (Dehnen 1973), image deformation, and rotation due to the lensing of the curved spacetime as well as other modifications in the phase wavefront, including gravitational Berry phase effects (Carini et al. 1992; Feng & Lee 2001; Yang & Casals 2014).

Light propagating near rotating black holes experiences a behaviour that is analogous to that experienced in an inhomogeneous anisotropic medium in a mechanism related to the Pancharatnam-Berry geometric phase (De Zela 2012). This involves spatially inhomogeneous transformations of the polarization vector in the observation plane of an asymptotic observer causing the lensed light to acquire OAM. The OAM present in that light can be univocally characterized by the so-called spiral spectrum (Torner et al. 2005), to be discussed more in detail in the methods section, revealing the rotation of the BH. Because of the properties of the Kerr metric, the OAM content in the EM radiation lensed by the Kerr black hole (KBH) and the associated spatial distribution of the azimuthal phase $\phi(\varphi)$, depend only on the observables inclination i of the KBH equatorial plane with respect to the observer and the rotation parameter $a = J_{\text{BH}}/(m_{\text{BH}}c)$, where J_{BH} is the KBH angular momentum, but not on the mass m_{BH} of the BH (Tamburini et al. 2011a).

Here we report the first observational confirmation of such GR-induced OAM vorticity, detected in the public brightness temperature data (EHT Collaboration 2019a) and also from the visibility amplitude and phase maps from Event Horizon Telescope (EHT) observations at $\lambda = 1.3$ mm of the central compact radio source surrounding a supermassive black hole M87* in the galaxy M87 of the Virgo Cluster released by EHT team (EHT Collaboration 2019b,c,d,e,f,g). Exploiting this OAM we were able to directly measure the spin, sense of rotation and inclination of M87*.

2 METHODS

The key tool to determine the BH rotation parameter a is the so called spiral spectrum. Torner et al. (2005) ideated this method that uniquely identifies the OAM content in the electromagnetic radiation, using the fundamental physical property that any light beam can be decomposed into a set of discrete orthogonal eigenmodes, each carrying its own well-defined OAM quantity and known geometry. A convenient choice is Laguerre-Gaussian modes. In cylindrical polar coordinates (ρ, φ, z) these paraxially approximate modes describe an EM field at z with amplitude (Barnett & Allen 1994)

$$u_{m,p}(r, \theta, z) = \sqrt{\frac{2p!}{\pi(p+m)!}} \frac{1}{w(z)} \left[\frac{r\sqrt{2}}{w(z)} \right]^l L_p^m \left[\frac{2r^2}{w^2(z)} \right] \exp \left[\frac{-ikr^2}{2R(z)} - \frac{r^2}{w(z)^2} \right] \exp \left[-i(2p+m+1) \arctan \left(\frac{z}{z_R} \right) \right] e^{-im\varphi}, \quad (1)$$

where m is the azimuthal index that describes the z component of OAM, i.e. the number of twists in the helical wavefront (the topological charge), p is the radial node number

of the mode, z_R is the Rayleigh range of the beam, $w(z)$ the beam waist, $R(z)$ the radius of curvature, L_p^m the associated Laguerre orthogonal polynomial, and φ the azimuthal phase of the beam. The decomposition of a beam into orthogonal modes will give the spectrum of OAM states carried by the EM wavefront, i.e. the spiral spectrum.

Thus, to estimate the rotation of M87*, this is, step by step, the procedure that we followed:

(i) Using KERTAP software (Chen et al. 2015) we simulated numerically different scenarios of an Einstein ring by varying the emission parameters of the AD, the inclination of the BH spin i , the BH rotation parameter a of a KBH. For each simulation we obtained, in the image plane of an asymptotic observer, the field intensity, polarization and phase distributions and determine the content of OAM from the spiral spectrum (Torner et al. 2005), relating the physical properties of the BH system to that of the OAM distribution (Tamburini et al. 2011a) with the asymmetry parameter q . This quantity is the ratio of the height of the $m = 1$ component with respect to the $m = -1$ one found in each spiral spectrum. If $q > 1$, then the rotation is clockwise, whilst $q = 1$ indicates no rotation and $q < 1$ counter-clockwise. This identifies the content of OAM in the field. From the results of the numerical simulations, from each AD model chosen in the simulations, we relate q with a fixed i by using polynomial interpolations.

(ii) From the EHT data we extract the intensity I and reconstruct numerically the spatial phase distribution P of the field in the image plane of an asymptotic observer by using well-known phase reconstruction techniques based on the Transport of Intensity Equation (TIE) (Barbero 2006; Schulze et al. 2012; Lubk et al. 2013; Ruelas et al. 2018; Kelly 2018) and build the spiral spectra.

(iii) We estimate the rotation parameter a from the comparison of the spiral spectrum of each numerical simulation with those obtained from EHT data by using the asymmetry parameter q (Torres & Torner 2011).

We can use this technique with OAM states to determine the rotation parameter a building up the spiral spectrum for the M87* Einstein ring because the radio source has been spatially resolved at 1.3 mm wavelength by the ~ 10000 km EHT radio-interferometric baseline. In this case, the wavefront is obviously not plane such as that emitted from a point-like source at infinity, even if the distance from the source to the Earth is $D = 54.8 \pm 2.6 \times 10^6$ light years ($D \sim 16.8$ Mpc). Hence, we can determine, within a good approximation, the OAM content in the wavefront from the OAM spectrum of the received radio waves. Furthermore, from the asymmetry parameter q of the observed OAM spectrum we can determine the sense and magnitude of the rotation of the M87* and its inclination, verifying the theoretical predictions made by Tamburini et al. (2011a).

As seen from Eq. [1], this spectrum of OAM states carried by the EM wavefront is obtained by Fourier transforming the EM field with respect to the azimuthal angle φ . Since our twisted-light/OAM method operates in angular momentum space and uses the additional information encoded in the phase of the OAM beam, it is complementary to methods based on analyses in configuration (φ) space, such as the analysis of the deviation from the circularity of the M87* shadow adopted by EHT team (EHT Collaboration

2019b,c,d,e,f,g; Bambi et al. 2019), a method that has so far not been able to yield any conclusive results. In fact, the geometry of the shadow in Kerr metric (Kerr 1963) and the radius of the photon ring (the photon capture radius) changes with the ray orientation relative to the angular momentum vectors with respect to that of a Schwarzschild BH. This results in a deformation of the circular shape of the black hole’s shadow that was not possible to be determined with the available data. This deformation, even if small ($< 4\%$), will be potentially detectable only with future EHT acquisitions (EHT Collaboration 2019b); the data released so far only allow EHT team to determine the inclination of the BH spin and the presence of a clockwise rotation, through the comparison of the experimental data with about 60,000 templates of the Einstein ring and BH shadow obtained from numerical simulations.

Moreover, our method makes use of the additional information encoded in the phase of the OAM beam characterized by the asymmetry parameter q of the spiral spectrum due to the vorticity induced by the Kerr metric and emitted by a slightly larger region of the Einstein ring surrounding the BH, as explained more in detail in Tamburini et al. (2011a) and in the Supplementary Material (SM). Let us follow our procedure.

(i) Numerical simulations of OAM from the Einstein ring of a KBH. As initial step in the analysis and interpretation of the EHT data, we build up, with the help of the freely available software package KERTAP (Chen et al. 2015), a set of numerical simulations describing several scenarios of black-hole accretion disks, as measured by an ideal asymptotic observer, to compare with the results of the analysis of the experimental data. The value of the rotation parameter varied in the interval $0.5 < a < 0.99$ clockwise and counter-clockwise and the inclination $1^\circ < i < 179^\circ$. For the AD of the Einstein ring we adopted a thermalized emission with $0.1 < \Gamma < 2$ power spectra, chosen in agreement with ALMA observations (Doi et al. 2013; EHT Collaboration 2019f) and a radial power law index that specifies the radial steepness of the profile, of $n_r = 3$; we also simulated synchrotron emission, Compton scattering, and bremsstrahlung. Regarding the AD model used to fit with the observations, as discussed by the EHT team in Ref. EHT Collaboration (2019g), we also find that, in any case, the image properties are determined mainly by the spacetime geometry. KERTAP provides a detailed description of the propagation of light in Kerr spacetime (Kerr 1963) with an error $\sim 10^{-7}$, in geometric units ($G = c = 1$) and OAM routines $\sim 10^{-12}$.

The OAM content is then numerically calculated from KERTAP output images and the Stokes polarization parameters (U, Q, V), analyzing the parallel transport of the electric field and the Pancharatnam-Berry geometrical phase with the vectorial field technique developed by Zhang et al. (2015) where the radiation emitted from the simulated Einstein ring is a fully polarized vectorial vortex beam propagating in free space in the z direction from the BH to the asymptotic observer. The resulting spatial distribution of the azimuthal phase $\phi(\varphi)$ of the radiation used to calculate the OAM and the associated OAM spiral spectrum are invariant with respect to the mass m_{BH} of the KBH and depend only on the parameters i and a (Tamburini et al. 2011a).

(ii) Analysis of EHT data with OAM techniques. In order to construct the spiral spectrum (Torner et al. 2005), it

is necessary to analyze, at each point in the image plane, the intensity (amplitude) and the phase and then calculate numerically the OAM content by interpolating the field with the different OAM modes described in Eq. 1. OAM beams are detectable and can be accurately characterized with interferometric techniques that directly measure amplitude, intensity and phase, as has been demonstrated experimentally in the radio domain (Thidé et al. 2007; Tamburini et al. 2011b, 2012).

Since these kind of data are not all available from the EHT observations, in order to obtain the spatial phase distribution, we had to reconstruct the evolution of the wavefront with the well-known non-interferometric technique based on the TIE method and reduced error procedure (Barbero 2006; Schulze et al. 2012; Lubk et al. 2013; Ruelas et al. 2018; Kelly 2018). The TIE equations (see Eq. 6 in SM par. 1.2) recovers the phase evolution between two or more consecutive intensity images of a stable source, in the paraxial approximation, when the source itself is spatially translated along the z -axis with respect to the observer. This is exactly what happens for when the images of M87* were taken, because of its relative motion with respect to the Earth (for more details see SM).

The two intensity and phase wavefront plots (see Fig. 1 in the main text and Fig. 1 and 2 in SM) have been reconstructed from two sets of two consecutive images of the Einstein ring of M87*. The two different observational runs of EHT are each separated by one day, the first being epoch 1 (5 and 6 April 2017), and the second being epoch 2 (10 and 11 April 2017). The data were obtained from 10 seconds of signal averaging as described in Refs. (EHT Collaboration 2019a,e,f,g). The M87* exhibited a modest source evolution between the two pairs of nights 5–6 April and 10–11 April and a broad consistency within each pair.

Moreover, the TIE method can be applied because the physical evolution of the M87* Einstein ring structure during the two different EHT observation runs, each separated by one day, in two 2 GHz frequency bands centered on 227.1 GHz and 229.1 GHz is negligible and the source can be considered stable as already stated in Refs. (EHT Collaboration 2019f; Doeleman et al. 2012). More precisely, the evolution of the source during the time interval between the two sets of pairs of days, was $< 5\%$ within an observation (EHT Collaboration 2019d,e). Relative to the object, each day is $2.8R_g c^{-1}$ long for a BH with mass $M = 6.5 \pm 0.2|_{\text{stat}} \pm 0.7|_{\text{sys}} \times 10^9 M_\odot$. This timescale is shorter than the crossing time of light of the source plasma and short compared to the decorrelation timescale of EHT simulations used to analyze the experimental results, $50R_g c^{-1}$ (EHT Collaboration 2019f). It was observed only a small evolution with a maximum of a few percent of difference between the two epochs, separated by five days (EHT Collaboration 2019g,a).

With the TIE method one can estimate the OAM content from the brightness temperature distributions reported in the images (Rybicki & Lightman 2004) and then the rotation parameter of the KBH as it were obtained from two different and independent acquisitions. The TIE method remains valid even though the shift s along z due to the motion of our planet around the Sun in the interval of one day appears to be enormous with respect to the wavelength because the phase profile of an OAM wave repeats in space with a re-

Table 1. Table of values of the asymmetry parameter q , obtained by dividing the height of the $m = 1$ by that of $m = -1$ components of the spiral spectra (see text and SM) of Kerr black holes neighborhoods with different rotation parameters $0.5 < a < 0.9$. Vs. the rotation parameter a for two sample inclinations $i = 17^\circ$ and $i = 46^\circ$ simulated with KERTAP. The rotation is clockwise and averaged over different accretion disk emission mechanisms characterized by $0.1 < \Gamma < 2$ power spectra. The error is $\sim 10^{-7}$. In agreement with EHT we choose $i = 17^\circ$ (and $i = 163^\circ$).

BH rotation parameter a	0.50	0.60	0.80	0.90
Asymmetry parameter q				
$i = 17^\circ$	1.295	1.320	1.356	1.391
$i = 46^\circ$	1.392	1.412	1.424	1.438

currence modulo λ . Moreover, the properties of OAM waves are not degraded when traveling in free space the distance s , which is only a small fraction of the distance from M87* to the Earth.

The correctness of our procedure that uses the relative translational motion of the Earth with respect to M87* is mathematically ensured by the Wold theorem, (Wold 1954; Anderson 1994) as explained in the SM.

(iii) Estimating the BH rotation parameter. The rotation parameter a can be estimated by comparing the asymmetry parameter q , given by the ratio of the OAM spectrum components $m = 1$ and $m = -1$, for any value of the inclination parameter $1^\circ < i < 179^\circ$ with step of 1° obtained from the numerical simulations and the values of q obtained from the analysis of EHT data of epoch 1 and 2. In Tab. 1 is reported an example of values of the parameter q obtained from the numerical simulations of the Einstein ring of a KBH for two values of the inclination parameter, $i = 17^\circ$, as indicated by EHT, and $i = 46^\circ$ obtained by varying the rotation parameter a . The variation of $i = 1^\circ$ can be adopted as indetermination in i as it induces a small change $\Delta q = 0.0012$ corresponding to $\Delta a \simeq 0.06$ compatible with the variation of a in its error interval. The spiral spectra reported in Fig. 1 obtained with the TIE imaging techniques reveal the presence of an asymmetric ring with clockwise rotation and a “crescent” geometric structure that exhibits a clear central brightness depression. This indicates a source dominated by lensed emission surrounding the black hole shadow.

From the analysis of the two data sets we obtain the asymmetry parameters $q_1 = 1.417 \pm 0.049$ for epoch 1 and $q_2 = 1.369 \pm 0.047$ for epoch 2. They yield an averaged asymmetry in the spiral spectrum of $\bar{q} = 1.393 \pm 0.024$ corresponding to $a = 0.904 \pm 0.046$ (see SM). The average value of the asymmetry parameter is compatible with that resulting from our numerical simulations, $q_{\text{numerical}} = 1.389$, for an Einstein ring with a radius of 5 gravitational radii, emitting partially incoherent light around a Kerr black hole.

The values of q indicate that the KBH can have an inclination of $i = 17^\circ \pm 2^\circ$, with the angular momenta of the accretion flow and of the black hole anti-aligned, showing clockwise rotation as described in Ref. (EHT Collaboration 2019f), where an error of 1° was reported. The preferred inclination mentioned above is alternatively equivalent to a magnetically arrested disk (MAD) scenario with an inclination $i = 163^\circ \pm 2^\circ$ and the angular momentum

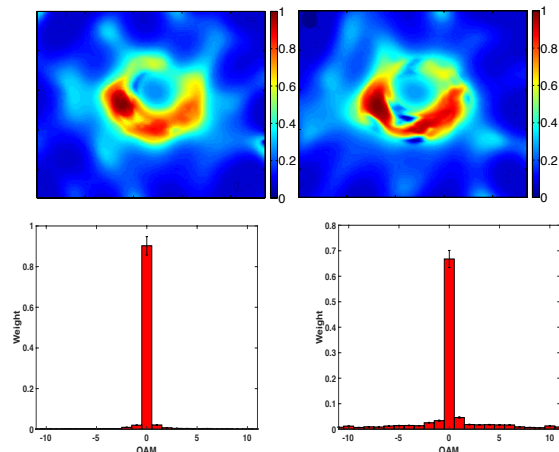


Figure 1. Experimental results. Normalized electric field component magnitudes along the observer’s direction reconstructed from the TIE analysis of the brightness temperature in a finite frequency bandwidth and for the corresponding spiral spectra for epoch 1 and epoch 2. The asymmetry q between the $m = 1$ and $m = -1$ components in both of the spiral spectra reveals the presence of twisted EM waves from the black hole Einstein ring (Tamburini et al. 2011a) with $a = 0.904 \pm 0.046$ rotating clockwise. The spin is pointing away from Earth and an inclination between the approaching jet and the line of sight of $i = 17^\circ$ if the angular momentum of the accretion flow and that of the black hole are anti-aligned (equivalent to a similar geometry with an inclination $i = 163^\circ$, but where the angular momentum of the accretion flow and that of the BH are aligned). The Einstein ring has gravitational radius $r = 5R_g$, as indicated by an EHT analysis dominated by incoherent emission (see EHT Collaboration 2019g,a, and text). The image coordinates are in arbitrary units. The intensity sidebars are normalized to unity.

of the accretion disk flow instead aligns with that of the black hole (Sob’yanin 2018). This is in agreement with the results of the EHT collaboration, presented and discussed in Refs. (EHT Collaboration 2019b,c,d,e,f,g). EHT analysis suggests that the X-ray luminosity is $\langle L_X 10^{-2\sigma} \rangle < 4.4 \times 10^{40}$ erg/s and the jet power is $P_{\text{jet}} > 10^{42}$ erg/s. The radiative efficiency is smaller than the corresponding thin disk efficiency (EHT Collaboration 2019f).

Our results above, obtained using the TIE methodology, show good agreement with those resulting from a more constraining approach, i.e. that which directly utilises the visibility amplitude and the phase maps for the day 11th April 2017 released by EHT. In particular, the EHT collaboration applied three data analysis methods: DIFMAP, EHT and SMILI, (EHT Collaboration 2019e,g,a). We obtained $q_{\text{DIFMAP}} = 1.401 \pm 0.047$, $q_{\text{EHT}} = 1.361 \pm 0.046$ and $q_{\text{SMILI}} = 1.319 \pm 0.045$, yielding for this day an averaged value of $\bar{q} = 1.360 \pm 0.027$ ($a = 0.821 \pm 0.062$). This value deviates by a quantity $\Delta a \simeq 0.087$ from that of epoch 2 obtained with the TIE method. Since, in all cases, it results $q > 1$, that confirms the presence of a clockwise rotation. The spiral spectra of this additional data analysis are reported in Figure 2.

The error in the final estimate of a depends on the numerical error of the TIE reconstruction method, $|\Delta a|_{\text{TIE}} \sim 10^{-7}$, and from that of the final EHT data products that include the calibrated total intensity amplitude and phase

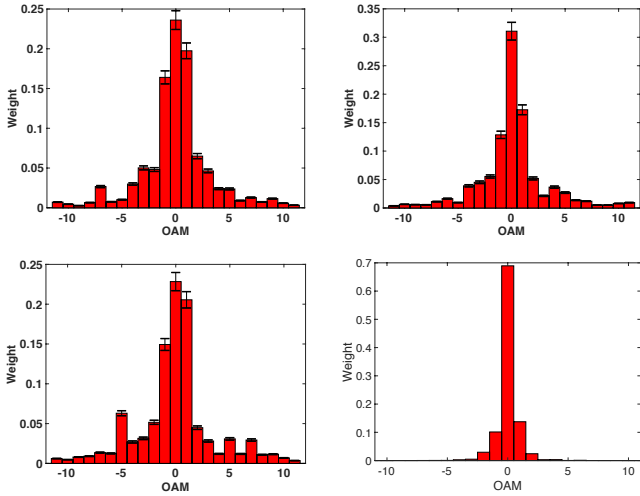


Figure 2. OAM spectra from the results of SMILI, EHT (up) and DIFMAP (bottom left) data analysis by EHT of the observation taken in 11 April 2017 (EHT Collaboration 2019e,g,a) and from the numerical simulations with KERTAP. The data considered here represent the visibility amplitude and phase, provided by EHT, as a function of the vector baseline. As the spatial phase distribution is, in this case, present in the data, we do not need to apply the TIE method to recover it. In all the data sets the asymmetry parameter, the ratio q between the $m = 1$ and $m = -1$ peaks in the spiral spectra, is $q > 1$ indicating clockwise rotation with $i = 17^\circ$ if the angular momentum of the accretion flow and that of the black hole are anti-aligned (equivalent to a similar geometry with $i = 163^\circ$, with angular momentum of the accretion flow and that of the BH are aligned). Bottom right, the value of q , obtained from the spiral spectrum of KERTAP simulations, has an error of $\sim 10^{-7}$ in agreement with the values found from these results and the TIE method.

information. The latter are validated through a series of quality assurance tests and show consistency across pipelines setting limits on baseline systematic errors of 2% in amplitude and 1° in phase giving a maximum error chi-squared test of $\sim 5\%$ (EHT Collaboration 2019b,c,d,e). By averaging for any point in the image the values in a neighborhood of three pixels we reduce the error in the calculation of the OAM spectrum $|\Delta a|_{\text{EHT}} \approx 0.046$. This ensures a good precision in the reconstruction of the surroundings of the BH and for our OAM analysis. The total error of a becomes,

$$|\Delta a|_{\text{tot}} = |\Delta a|_{\text{TIE}} + |\Delta a|_{\text{EHT}} \approx 0.046, \quad (2)$$

hence yielding a first conservative estimate of the rotation parameter at $a = 0.904 \pm 0.046$, with $\sim 95\%$ c.l. and the hypothesis of a static BH is excluded at $\sim 6\sigma$. More details can be found in the SM.

Even if the spatial phase profile was not measured directly for the values of q obtained with the TIE method, something that can be achieved with interferometric or other more direct techniques, the values of the rotation parameter a obtained with the OAM method agrees with the experimental data obtained from results presented in the literature. Preferably, one should take a succession of snapshots with the EHT at much shorter time intervals, typically a few minutes rather than days, to improve the accuracy of the terms in the TIE of Eq. 6 in the SM. This could be realized quite straightforwardly.

With dedicated observations and new fiducial pipeline

images of amplitude and phase plots, and new interferometric methods that analyze the EM field in intensity and phase (readily realized with standard radio telescopes as was reported for the fiducial pipeline images of the visibility amplitude and phase plots for 11 April 2017), one should be able to drastically improve the measurements of the OAM content within the spiral spectrum of the EM radiation emitted in the neighborhood of rotating black holes. As second step, it will be possible to estimate in a more accurate way the BH rotation and the other fundamental parameters of the system from the shape of the shadow. Ultimately, radio telescopes equipped with antenna systems optimized to directly capture and resolve the EM angular momentum in the signals received should be able to unleash the full potential of the OAM in observational astronomy. One advantage of involving OAM in black-hole astronomy is that polarization and OAM together build up the total angular momentum invariant \mathbf{J} and when polarization is affected by the presence of polarizing media such as dust and unstructured plasma, OAM will be less affected and can be used as a reference point to extract additional information about the source from its emitted light.

3 CONCLUSIONS.

Exploiting the properties of the Kerr metric, we were able to measure the rotation of M87* by analysing a sequence of images acquired by the Event Horizon Telescope. In particular, the estimate of the rotation parameter a was derived from the characterization of the vorticity of the electromagnetic waves emitted from the surroundings of the BH, affected by a strong gravitational lensing from the rotating compact object (Tamburini et al. 2011a). The OAM and the electromagnetic vorticity were reconstructed from the public released images of the brightness temperature of the Einstein ring of the M87 black hole, taken during four different days with a well-known technique based on the Transport of Intensity Equation (Rybicki & Lightman 2004; Lubk et al. 2013; Zhang et al. 2015) that permits the reconstruction of the phase wavefront and of the orbital angular momentum content from two or more consecutive acquisitions of the same source taken at different distances.

By applying the general relativistic effect in the Kerr metric discussed in (Tamburini et al. 2011a), we find that the central black hole in M87 is rapidly rotating clockwise with rotation parameter $a = 0.90 \pm 0.10$ and inclination $i = 17^\circ \pm 2^\circ$ (equivalent to a magnetic arrested disk with inclination $i = 163^\circ \pm 2^\circ$) with 95% c.l. and the case for a non-rotating BH is excluded with $\sim 6\sigma$ c.l.. This enormous amount of energy trapped in the black hole rotation implies a rotational energy of about 10^{64} erg, comparable to the energy emitted by the brightest quasars over Gyr timescales (Christodoulou & Ruffini 1971).

ACKNOWLEDGEMENTS

We thank Guido Chincarini for help and useful discussions. FT. acknowledges ZKM and Peter Weibel for the financial support. The encouragement and support from Erik B. Karlsson is gratefully acknowledged.

Supplementary Material:

4 OAM/PHASE RECONSTRUCTION METHODS FROM NUMERICAL SIMULATIONS AND EXPERIMENTAL DATA

The reconstruction of the phase profile from phase-front intensity patterns is a novel non-interferometric technique. It is based on the Transport of Intensity Equation (TIE) method that requires a careful mathematical and numerical analysis of the problem (Lubk et al. 2013; Ruelas et al. 2018). In our case we limit our analysis to paraxial optics. In principle, the TIE method requires only two or more spatial intensity distributions (images) from a field intensity acquisition system, exactly as was made by the Event Horizon Telescope (EHT) collaboration.

In fact, the EHT collaboration took a series of radio “snapshots” at different times. Because of the relative motion in space of the Earth and M87*, as if the whole acquisition system were mounted over an movable optical translation stage, the different observations were made at different distances from the source. This relative motion gave rise to a translation in space that is enormous in terms of wavelengths ($\lambda = 0.0013$ metres, 230 GHz). Even so, the TIE method can still be applied thanks to the following:

- The source was stable during the acquisitions that were separated by one day in each of the two different observation epochs.
- The scattering due to interstellar matter did not affect the propagation of the radio waves from M87* to the Earth.
- The optimization procedure adopted for the image reconstruction minimised acquisition errors during the observations.
- The Einstein ring observed around M87* had a simple structure.

These fortuitous conditions ensure that the results of the excellent image reconstruction process used by EHT team are good enough to allow a reliable determination of the spatial phase distribution, enabling the estimation of the black hole (BH) rotation parameter from an analysis of the spiral spectrum components.

4.1 Reconstruction of the spatial phase distribution from Stokes and Pancharatnam–Berry phases

The KERTAP software package (Chen et al. 2015) describes the spacetime geometry around a rotating Kerr black hole (Kerr 1963) and calculates the gravitational optics phenomena such as lensing and polarisation. Here we describe how to use KERTAP to calculate the radio orbital angular momentum induced by the Kerr black hole rotation.

We calculate the expected phase pattern of an Einstein ring for different values of the rotation parameter, i.e. the angular momentum per unit mass ($a \leq 1$), of the BH that, together with the BH mass m_{BH} , is described in Boyer–Lindquist coordinates in geometric units ($G = c = 1$) by the Kerr space-time in the cylindrical coordinate system

$(t, r, \vartheta, \varphi)$

$$ds^2 = \frac{\rho}{\Delta} dr^2 + \varrho^2 d\vartheta^2 + \frac{\sin^2 \vartheta}{\varrho^2} \left[a dt - (r^2 + a^2) d\varphi \right]^2 - \frac{\Delta}{\varrho^2} (dt - a \sin^2 \vartheta d\varphi)^2 \quad (3)$$

where

$$\varrho^2 = r^2 + a^2 \cos^2 \vartheta \quad (4)$$

and

$$\Delta = r^2 - 2m_{\text{BH}}r + a^2 \quad (5)$$

The OAM of the EM field emitted from the M87* surroundings is induced by the gravitational lensing of the rotating black hole and its rotation. To characterize the rotation parameter obtained from the analysis of the EHT data, we numerically simulate the gravitational lensing around different BHs with different inclinations and rotation parameters. Then we reconstruct the spatial phase profile from the Stokes parameters (polarisation) provided by KERTAP and from the calculation of the Pancharatnam–Berry phase. An example is shown in figure 3.

In the paraxial approximation, the electric field vector of the received beam can be written as [cf. Eq. (1.5) in Ref. (Allen & Padgett 2011; Zhang et al. 2015)]

$$\mathbf{E}(x, y) = i\omega \left[u_x \hat{\mathbf{x}} + u_y \hat{\mathbf{y}} + \frac{i}{k} \left(\frac{\partial u_x}{\partial x} + \frac{\partial u_y}{\partial y} \right) \hat{\mathbf{z}} \right] \exp(ikz) \quad (6)$$

where u_x , u_y and u_x^* , u_y^* represent the complex amplitudes of the x and y components and their complex conjugates, respectively, of the electric field in the image plane. The quantity ω is the angular frequency, and k is the wave number.

In SI units the z component of the EM orbital angular momentum density is (Thidé et al. 2014)

$$\varepsilon_0 [\mathbf{x} \times (\mathbf{E} \times \mathbf{B})] \cdot \hat{\mathbf{z}} = \frac{\varepsilon_0}{2\omega} \sum_{i=1}^3 E^* \hat{L}_z E_i = \frac{\varepsilon_0}{2\omega} \sum_{i=1}^3 E_i^* \left(-i \frac{\partial}{\partial \varphi} \right) E_i$$

where $\mathbf{x} = x\hat{\mathbf{x}} + y\hat{\mathbf{y}} + z\hat{\mathbf{z}}$ is the radius vector from the source to the observer. Then, one obtains the z component of the EM angular momentum, expressed in terms of the complex amplitudes of the x and y components of the field as (Zhang et al. 2015)

$$\hat{L}_z = i \frac{\omega}{2} \left(u_x \frac{\partial u_x^*}{\partial \varphi} + u_y \frac{\partial u_y^*}{\partial \varphi} - u_x^* \frac{\partial}{\partial \varphi} - u_y^* \frac{\partial}{\partial \varphi} \right). \quad (7)$$

Taking the Stokes parameters (I, U, V) for the linear and elliptic polarisation states as reference fields, the Pancharatnam–Berry phase of the vortex field $\mathbf{E}(x, y)$ that we want to determine is given by the quantity (Zhang et al. 2015)

$$\psi_{P(V/U)} = \arg(\langle \Phi_V | \Phi_E \rangle) \quad (8)$$

More precisely, $\psi_{P(V/U)}$ is calculated with the argument of the ratio between the circular/elliptic state of polarisation of the EM field, characterized by the Stokes parameter V , and the state $|\Phi_V\rangle$, and that of the initial field $\mathbf{E}(x, y)$, namely, $|\Phi_E\rangle$.

According to Zhang et al. (2015), one obtains the average value of the OAM topological charge m of the field, for any concentric circle of pixels having radius r_c and with the

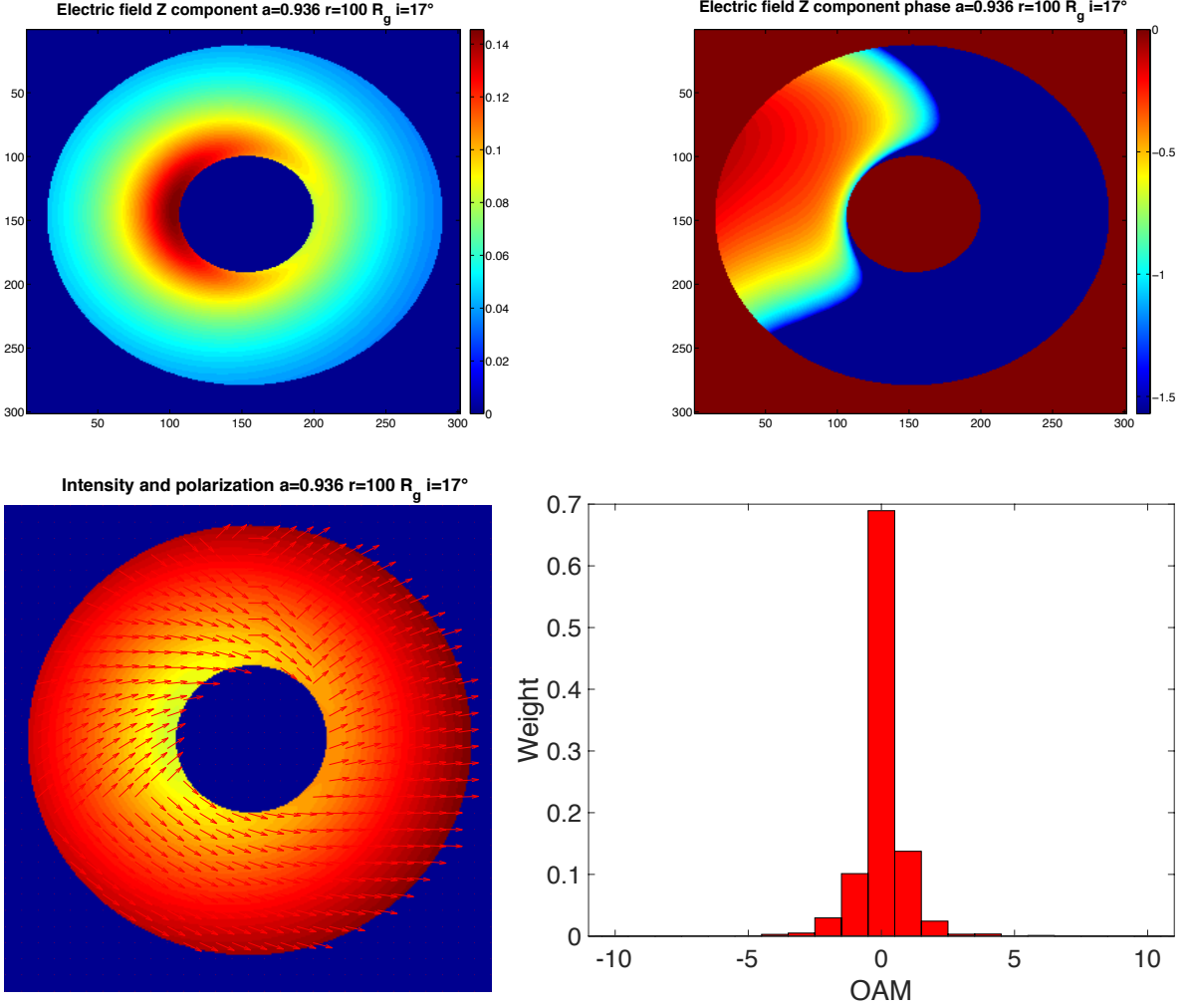


Figure 3. Results of numerical simulations from KERTAP Upper panels: Intensity, normalised to unity (left), and phase (right) of the z component of the radiation field emitted from the black hole accretion disc dominated by thermalised emission and synchrotron radiation. The black hole has a spin pointing away from Earth and an inclination between the approaching jet and the line of sight of $i = 17^\circ$. This is equivalent to a similar geometry with an inclination $i = 163^\circ$ for a magnetic arrested disk (van Putten 1999; van Putten & Ostriker 2001), but where the spin is aligned with the accretion flow pointing toward the Earth. Polarization and spiral spectrum plots are shown in the lower panels. This geometry, shown here at an orientation of 90° , agrees with that described by the experimental spiral spectra showing clockwise rotation as discussed in the main text, in agreement with the asymmetry parameter q , the ratio between the $m = 0$ and $m = 1$ peaks (OAM amplitudes) of the experimental data. This is smaller than that generated by the theoretical model, showing lower coherence in the emission mechanisms. The error is on the order of 10^{-7} and errorbars are not reported here.

origin at the center of the image, from

$$\frac{\partial m}{\partial \varphi} = r_c I_N \left(-I \frac{\partial \psi_{P(V/U)}}{\partial \varphi} \mp (I \pm U) \frac{\partial \psi_s}{\partial \varphi} \right). \quad (9)$$

This quantity is implemented numerically in the plane of observation of an asymptotic observer. In Eq. 9 the quantity I_N is the normalised intensity. The first term, $I \partial(\psi_{P(V/U)})/\partial \varphi$, is the gradient of the spiral spatial phase distribution obtained from the Stokes parameters V and U . Finally, the term $(I \pm U) \partial \psi_s / \partial \varphi$, describes the variation of the state of the polarisation in space at each point in the observational plane of the asymptotic observer. At the end one can calculate the spiral spectrum.

4.2 Reconstructing the spatial phase distribution from different intensity acquisitions

Here we describe how we determined the rotation of the M87* black hole from the brightness temperature distributions (Rybicki & Lightman 2004) provided by EHT, by using the Transport of Intensity Equation (TIE) method (Barbero 2006; Schulze et al. 2012; Lubk et al. 2013; Ruelas et al. 2018; Kelly 2018), adopting a finite-difference method for a series of matrices (250×250) of intensity values.

As described in the standard literature, the OAM of the EM field can be determined from the spatial phase distribution and the spatial intensity (or amplitude) distribution in the plane of observation of an interferometer (Tamburini et al. 2011b). If the spatial phase distribution is not available it can be reconstructed with the TIE method. To explain

this procedure better, let us consider the intensity of the EM field as in Eq. 6; the EM waves are described in terms of complex-valued terms of the amplitude $u(r)$ in the following paraxial wave equation (Goodman 1996; Ruelas et al. 2018, see)

$$\left(\nabla_{(x,y)} \cdot \nabla_{(x,y)} + 4\pi i \frac{\partial}{\partial z} \right) u(r) = 0 \quad (10)$$

where $\nabla_{(x,y)}$ represents the vector nabla differential operator in the image plane (x, y) perpendicular to the z axis connecting the BH and the asymptotic observer.

By multiplying equation (10) with its complex conjugate, one can split this equation into a system of partial differential equations (the system of TIE equations) that describe the intensity and the phase evolution with respect to the translational motion across the z axis as explained in Ref. (Ruelas et al. 2018),

$$\frac{\partial I}{\partial z} = -\frac{1}{2\pi} \nabla_{(x,y)} \cdot (I \nabla_{(x,y)} P) \quad (11a)$$

$$\frac{\partial P}{\partial z} = \frac{1}{4\pi\sqrt{I}} \nabla_{(x,y)}^2 \sqrt{I} - |\nabla_{(x,y)} P|^2 \quad (11b)$$

Here, I is the intensity and P the phase distributions in the plane of propagation that evolves along the z coordinate. We solve numerically this system of equation point by point in the image plane, for given values of I , and recover P . The evolution of the phase P and intensity I along the z axis – connecting M87* and the Earth – is provided by the relative motion of the Earth with respect to M87 occurred between each different acquisition.

The quantity $|\nabla_{(x,y)} P|$ is the magnitude of the phase gradient vector in the image plane. To summarise, by using the numerical solution of the system of equations 11a in the image plane of an asymptotic observer, we reconstruct the spatial phase distribution from the intensity plots provided by EHT and determine the rotation from the analysis of the OAM spiral spectrum. The asymmetry parameter q given by the ratio between the $m = 1$ and $m = -1$ components (amplitudes) of the OAM spiral spectrum the histogram is compared with the values of q obtained from the numerical simulations performed with KERTAP. Then, using Matlab, we obtained the rotation parameter a by a polynomial interpolation of a as a function of q obtained by varying the inclination parameter i for any type of accretion disk. As discussed also by the EHT team in their numerical simulations EHT Collaboration (2019g), we also find that the image properties are determined mainly by the spacetime geometry, that are dominant, and then by the AD characteristics.

4.3 Applicability of the TIE method

As discussed in the main text, the EM waves at 230 GHz propagate unaffected by the scattering, e.g. due to the interstellar medium and other astrophysical effects (Tamburini et al. 2011c) from M87* to the Earth. The propagation of these EM waves remains quite stable also during the relative motion of the source with respect to the observer during the time interval of one day that separates two consecutive intensity acquisitions in each of the two acquisition epochs. To give an estimate of the relative shift between M87* and the receiving radiotelescopes, one has to consider that the relative motion of M87 is due to an heliocentric radial ve-

locity $v_{\text{rad}} = 1282 \pm 7$ km/sec and the source is located at a distance of $54.8 \pm 2.6 \times 10^6$ light years (ly) (Cappellari et al. 2011; NED 2019). The ratio between the total propagation distance from M87* to the Earth and that due to their relative motion in one day is very small

$$\frac{\Delta L_{\text{day}}}{\Delta L_{\text{tot}}} \approx 2.5 \times 10^{-12}. \quad (12)$$

The change of the EM wavefront from M87* in one day of motion is then due mainly to the phase profile of the wavefront, namely due to the presence of OAM. In fact, the propagation of EM waves at that frequency cannot be affected by possible astrophysical effects in the spatial interval traveled by the Earth with respect to M87* during one day. The explanation is quite trivial: this distance is extremely small with respect to the total distance from M87* and our planet and there are not extreme astrophysical phenomena around the Earth's orbit that can affect the propagation of light (Tamburini et al. 2011c). The small deviations observed are due to acquisition/instrumental errors and from the unknown remainder modulo λ separating the two acquisitions of each of the two observational epochs. This quantity can be handled as a stochastic term in the determination of a . The mathematical validity of our procedure based on the TIE method is ensured by the Wold theorem described below.

5 THE WOLD THEOREM

Wold's decomposition (or representation) theorem states that every covariance-stationary time series Y_t or, equivalently, the time evolution of a discrete process in time, can be decomposed into a sum of two time series: one deterministic time series and a stochastic one.

The time-discrete process that we consider here is represented by the evolution of the brightness temperature value Y_t in each image pixel at the position (x, y) of the BH image and at the time t of observation. The evolution of Y_t is a time series that can be described in terms of covariance-stationary time series because the physical variations observed in M87* are very small, as reported in Refs. (EHT Collaboration 2019f; Doeleman et al. 2012). By applying the Wold theorem this process can effectively be approximated and modeled as a sum of a deterministic process plus a stochastic deviation, in which all the terms of the sequence have the same mean, and the covariance between any two terms of the sequence depends only on the relative positions of the two terms.

The deterministic part represents the slow temporal evolution of M87*, which is a quasi-static source (EHT Collaboration 2019e,f,g), when observed in the intervals of one day that separate the acquisitions of each of the two pairs of nights (5–6 April and 10–11 April) with a broad consistency. The stochastic deviation from the deterministic part, on the other hand, is given by the contribution of the undetermined variation modulo the wavelength λ that occurs during the long translational motion of a terrestrial observer with respect to the source, M87 and from the experimental errors.

The phase is reconstructed with the help of the TIE method, which is always a deterministic process that approximates an ideal time series of events described in the

interval $0 \leq t < \infty$ by the sequence

$$Y_t = \sum_{j=0}^{\infty} b_j \epsilon_{t-j} + \eta_t \quad (13)$$

where ϵ_t is an uncorrelated sequence. The innovation process ϵ_t ¹ can be represented by a white noise process. The terms b_j act as linear filters and are constant in time. The vector b is essentially the coefficient vector of the stable stochastic process, and η_t is the information encoded in the images, namely, the field amplitude or the intensity in each of the acquisitions. Any stationary process such as our phase reconstruction process can be described with a good approximation by this particular representation.

The dynamical evolution of any process with these properties can be approximated by a linear model and if all the stochastic processes are independent, this is the only linear representation possible of this process, especially when the stochastic process is small with respect to the deterministic process. As described by Ruelas et al. (2018), the TIE analysis can unambiguously extract all the information encoded in the two (or more) different images. In fact, introducing a stochastic noise in the variable u , and thus in the intensity I the system of equations 11a becomes equivalent to a system of stochastic differential equations that can be solved numerically in a domain where the sum of the effective value of the brightness temperature and of the stochastic process are different from zero. This condition is always satisfied in the values of the brightness temperature in the EHT images of M87*. This proves the mathematical consistency of the TIE method in our approach of estimating the spatial phase distribution.

6 SPIRAL SPECTRA AND BH ROTATION: ADDITIONAL MATERIAL

To proceed with the analysis of the BH rotation one must obtain a reference OAM (spiral) spectrum from a set of numerical simulations of an Einstein ring. Then, one has to characterize the OAM content in the simulated image from the analysis of the amplitude (or intensity) and the phase of the field in the image plane of an asymptotic observer. As explained in the main text, the asymmetry of the OAM states $m = 1$ and $m = -1$ indicated by the heights in the columns of the histogram of the spiral spectrum allows us to estimate, with good accuracy, the twist in the light due to the rotation of the BH.

The ratio q between the height of the $m = 1$ and $m = -1$ column peaks (OAM amplitudes) in the spiral spectrum for an Einstein ring as observed in M87* if, in the simulations, we assume a photon power law index in the range $0.1 < \Gamma < 2$. We concentrate our efforts on the canonical case (Falcke & Biermann 1995) $\Gamma = 2$ and assume a radial power law index that specifies the radial steepness of the profile, namely, $n_r = 3$.

¹ The innovation process is the difference between the observed value of a variable at time t and the optimal forecast of it, based on information available prior to t . If the representation of the stochastic process is correct, any successive innovation results are uncorrelated and innovations are modeled with a white noise time series.

We present the plots of the field amplitudes and the z phase for the observational epochs discussed in the main text, epoch 1 (SM Fig. 4), and epoch 2 (SM Fig. 5).

6.1 Coherence of the EM waves and the TIE method

In the spiral spectra plots of Fig. 1 and Fig. 2 in the main text, and in Fig. 2, of the SM, we notice that the ratios between the $m = 0$ and $m = 1$ modes obtained with the numerical simulations are slightly different from those obtained with the visibility intensity and phase plots and different from those obtained from the TIE method.

If we describe the system with a theoretical model with a photon power law index $\Gamma = 2$ and a radial power law index $n_r = 3$, one obtains the amplitude ratio $q = h(m = 0)/h(m = 1) = 7.6$, whereas the experimental data analysed with the TIE method we find for epoch 1 (days April 5–April 6) that the ratio $h(m = 0)/h(m = 1) = 14.65$ and for epoch 2 (days April 10–April 11) that the ratio $h(m = 0)/h(m = 1) = 13.95$. This discrepancy suggests that the numerically simulated source has higher coherence than that found in the experimental data. Anyway, we notice that in both epochs the ratio between the two $m = 0$ and $m = 1$ modes of the experimental data are quite stable.

The difference between the theoretical and experimental results can be attributed to the concomitance of two main effects: (1) the experimental source can be more thermalised/scattered than what is assumed in the theoretical model, suggesting that the emission from the source has less coherence; (2) if this loss of coherence depends on the time of separation between two consecutive acquisitions, our results could have been improved by reducing Δt that now is on the order of one day. Of course, the acquisition of several snapshots and the reduction Δt would give more information about the natural coherence of the source emission mechanism.

What is important in the estimation of the rotation parameter a is not the coherence of the source (Shvedov et al. 2005) but that the asymmetry between the $m = 1$ and $m = -1$ modes remain stable. This property has been observed both in the numerical simulations and with the experimental results. The ratio between the $m = 0$ and the peaks $m = \pm 1$ are not crucial to determine a . This suggests that the method we used is a promising way to determine the twist of electromagnetic waves due to the rotation of the BH directly from the experimental data.

In fact, a better result could be obtained with a fast imaging technique, involving all EHT radio telescopes, to build up a series of consecutive snapshots. These images would be characterized to have a short coherence time due to atmospheric phase fluctuations that can occur on timescales of tens of seconds. This technique could be easily implemented in future EHT observations, with the experimental acquisition of the azimuthal spatial phase profile of the source, centered on the BH shadow, obtained with interferometric techniques. An antenna and data acquisition system designed for direct measurement of OAM would open entirely new avenues in astronomy and space sciences and technology in general.

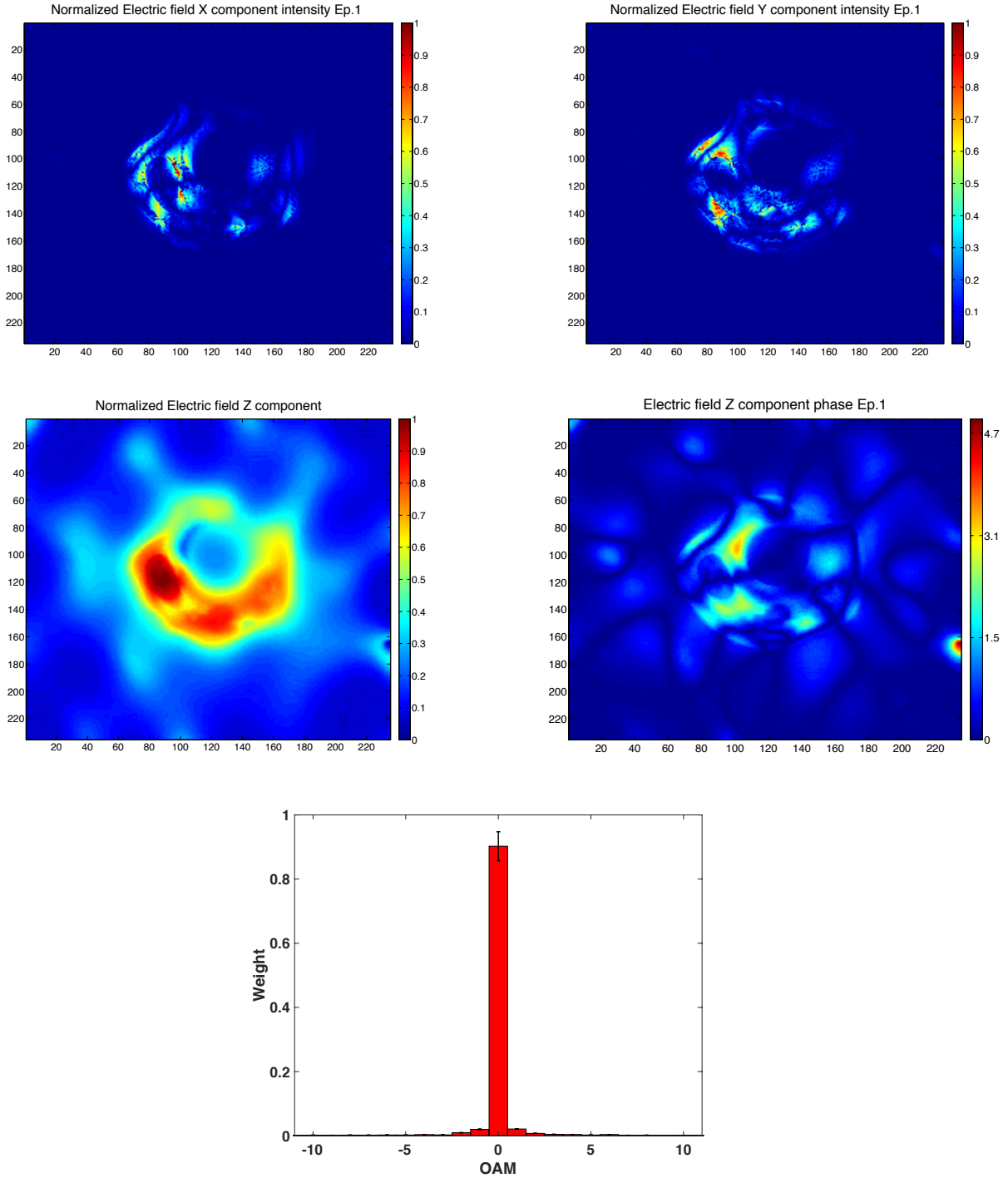


Figure 4. **Upper panels:** Normalised electric field x (left) and y component (right) reconstructed from the two EHT data acquisitions taken during epoch 1 (April 5 and 6, 2017, respectively), with the Transport of Intensity Equation (TIE) method. **Lower panels:** Normalised electric field intensity and phase across the direction of observation z and the corresponding spiral spectrum. The spiral spectrum shows the presence of a black hole rotating clockwise with rotation parameter $a = 0.90 \pm 0.10$ and inclination 17° pointing away from Earth (see main text). The TIE reconstruction method of the fields is possible because the M87 black hole Einstein ring is spatially resolved by EHT. The wavefront reconstructed here is not plane and therefore different from that emitted from a point-like source at infinity. The EM fields can be described as an unguided transverse magnetic (TM) beam in free space (Davis & Patsakos 1981). The image coordinates are in arbitrary units. The intensity sidebars are normalised to unity. The phase sidebars are in arbitrary units.

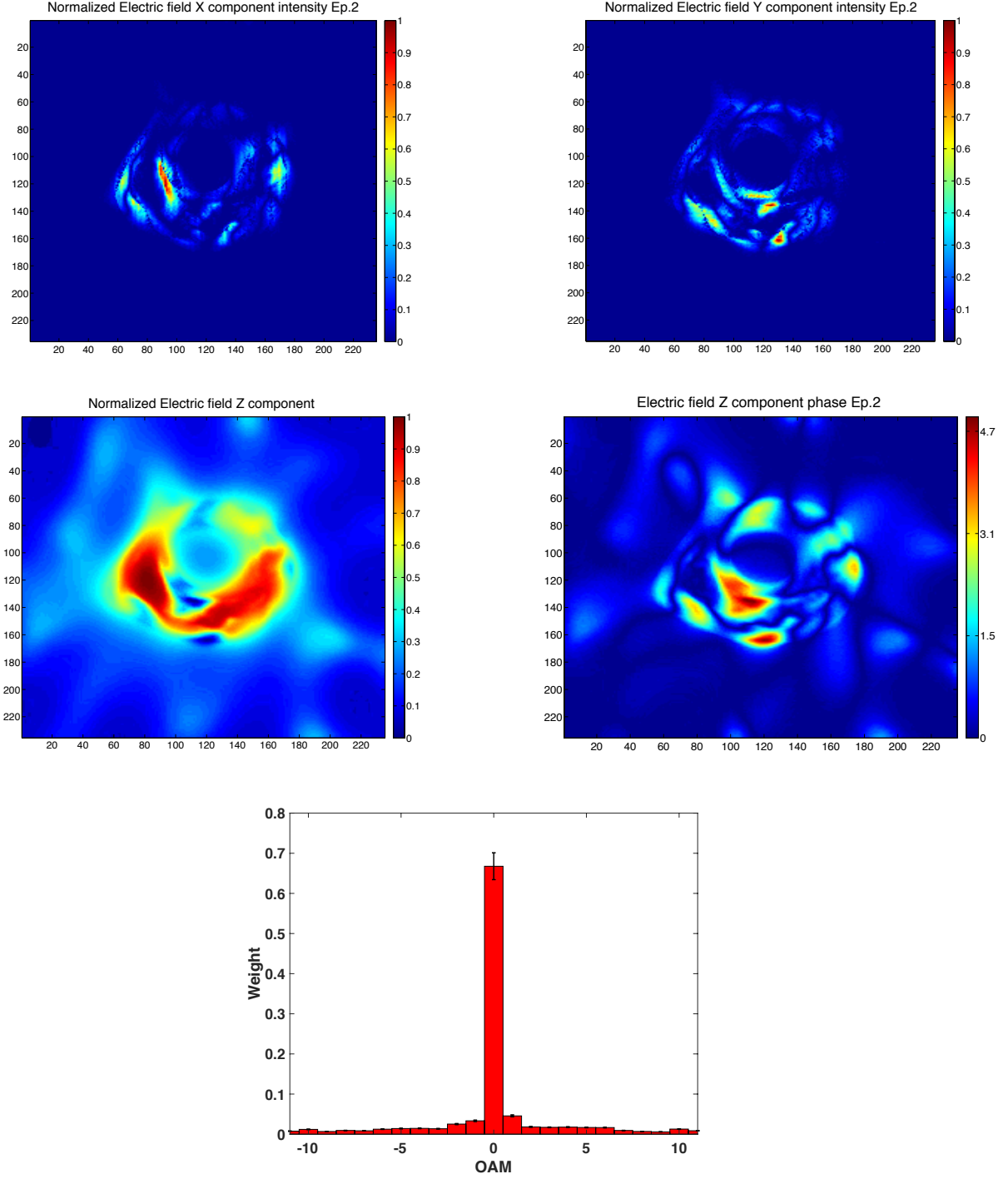


Figure 5. Epoch 2. Field components and spiral spectrum obtained with the TIE method as in SM Fig. 4. Also here, the spiral spectrum, as in epoch 1 that the component of the electromagnetic field along the propagation direction to the observer, agree with the results of a twist in the light caused by a clockwise rotating black hole with rotation parameter $a = 0.90 \pm 0.10$ as previously discussed (see main text). The image coordinates are in arbitrary units. The intensity sidebars are normalised to unity. The phase sidebars are in arbitrary units.

6.2 Calculating the error in the rotation parameter a

We calculate the total error in the determination of the rotation parameter a by applying the error propagation theory. To estimate this error one has to estimate first the error

in the spatial phase distribution on the image plane of an asymptotic observer from the TIE equations and from the error in the estimation of the intensity I . The I error in each of the EHT images of M87 is obtained through the convolution of different intensity patterns by using the NMF (negative matrix factorization) reconstruction method to reduce

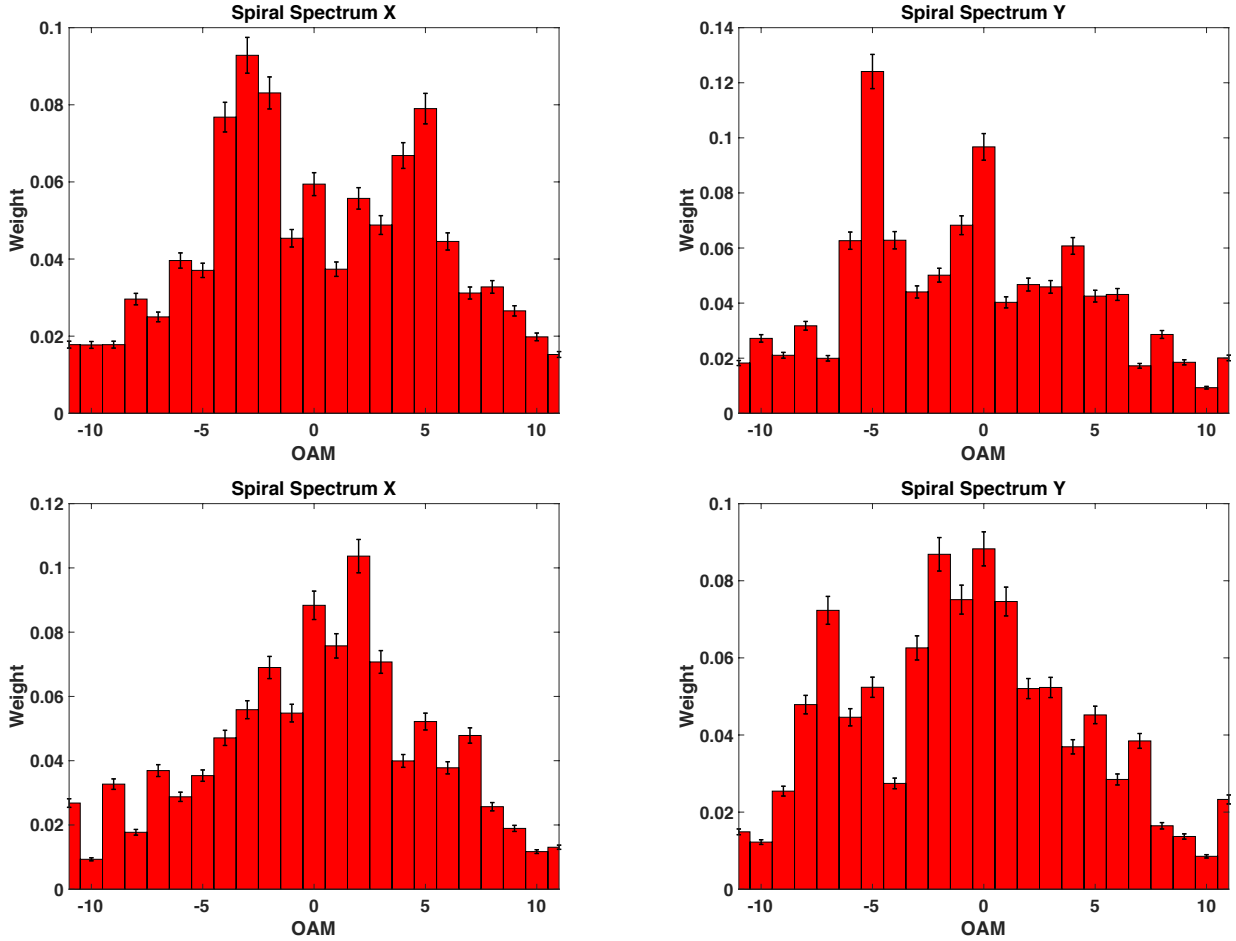


Figure 6. Upper panel: Spiral spectra of the x and y components of the electric field, obtained with the TIE method from EHT data in epoch 1 and those in epoch 2 (**Bottom panel**). Both components in both epochs do not show a predominant OAM component, as expected.

the error in agreement with the chi-squared (χ^2) test from EHT team. This procedure ensures a high-quality image construction process, with an estimated error in the pattern of 5%. The uncertainties are quantified in units of brightness temperature, with an error confidence interval of 95% (EHT Collaboration 2019e). Thus, all the images provided by the EHT collaboration satisfy a 5% maximum error chi-squared test that is the maximum error we assume for EHT data $|\Delta a|_{EHT}$ in the determination of the intensity spatial distribution. In summary, all the images provided by the EHT scientific documentation are presented and discussed in Refs. (EHT Collaboration 2019b,e,f,g).

As we adopted the numerical approach to solve the TIE equations, the error is calculated numerically. In fact, a complete analytic approach to obtain an exact formulation of the error distribution needs, of course, the analytic solution to the system of equations 11a. This seems not to be possible but for special cases where the intensity distribution patterns are circular, as discussed in Ref. (Ruelas et al. 2018). The error in the spatial phase distribution $P(x, y)$ is mainly due to the experimental errors present in the EHT data. This error affects the OAM and the spiral spectrum and is determined numerically by varying, in the input of the TIE routines, the intensity distribution I with its error interval

obtained from public EHT data. From this we obtain the error in the the spiral spectra, as reported in the figures 4-6. Then we obtain the error in the estimation of the asymmetry parameter q .

The error in the estimation of the parameter a depends on the numerical error of the TIE reconstruction method, $|\Delta a_{TIE}|$, and from the error deriving from the final EHT data products, $|\Delta a_{EHT}|$. The latter term is obtained numerically by varying q in its error interval with the polynomial relationship found between the asymmetry parameter q and the rotation parameter a .

We conservatively assume that the final uncertainty of a is given by the sum of the absolute values of the two errors, the first from the numerical errors introduced by the routines used to calculate the OAM spectrum ($\sim 10^{-12}$) and the polynomial interpolation $|\Delta a_{TIE}| \sim 10^{-7}$, which can be considered negligible, and the second, which is due to the error derived from the analysis of the experimental data provided by EHT and then processed by our numerical routines.

As already mentioned, the other term $|\Delta a_{EHT}|$ is calculated numerically. To improve the estimate of the parameter a and lower the associated error, we reduced the maximum error $\sim 5\%$ given in the data released by EHT in the following way: for each point $P(x, y)$ in any of the data images of

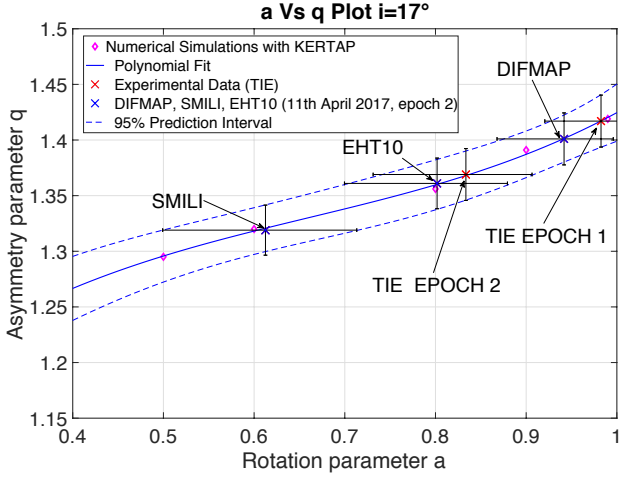


Figure 7. Plots of the rotation parameter a vs. the asymmetry parameter q for $i = 17^\circ$. The values of the rotation parameter a obtained from the TIE method, and from the visibility amplitude and phase maps from the observations on 11th April 2017 obtained by EHT with the image processing reduction methods (DIFMAP, SMILI and EHT), are in good agreement. They indicate the presence of a disk with inclination $i = 17^\circ$ (or equivalent to $i = 163^\circ$) with $\sim 95\%$ confidence interval.

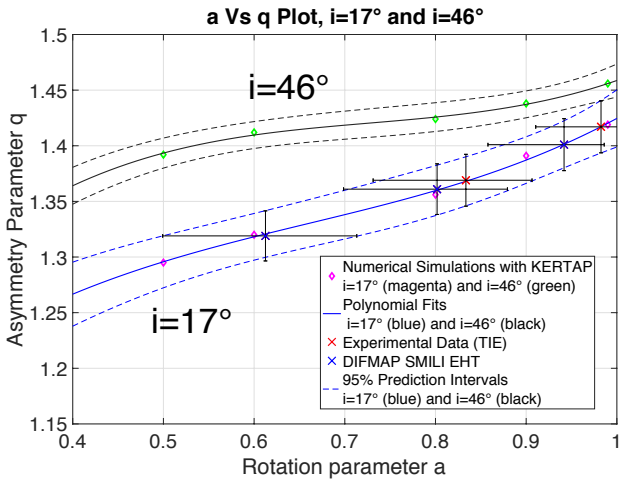


Figure 8. Plots of the interpolations of the rotation parameter a vs. the asymmetry parameter q for $i = 17^\circ$ and $i = 46^\circ$ with their $\sim 95\%$ confidence intervals. The experimental data, presented in Fig. 7, favour the conclusion of an inclination of $i = 17^\circ$. Overlapping between the two curves and respective 95% confidence intervals are not observed.

the M87*, we extract the value of the brightness temperature in P (which is equivalent to the intensity of the field I) and those of the adjacent points in a neighborhood of a chosen set of N pixels, $P(x \pm n, y \pm n)$, where $n \in [1, \dots, N]$. For the sake of brevity, we call these intensities I_j . Then, we

calculate the average at $P(x, y)$ and the variance

$$\bar{I}_{x,y} = \frac{1}{N} \sum_j I_j \quad (14a)$$

$$\sigma_{\bar{I}_{x,y}}^2 = \frac{\sum_j \sigma_j^2 + 2 \sum_i \sum_{k < j} \text{cov}(X_j, X_k)}{N^2} \quad (14b)$$

If we assume that the I_j 's are independent and identically distributed (iid) random variables, then the respective covariances are zero and we obtain $\sigma_{\bar{I}_{x,y}}^2 = \frac{\sum_j \sigma_j^2}{N^2}$. This procedure has been adopted in the numerical routines that are used to calculate the OAM spectrum and thus the asymmetry parameter q also for the the spatial phase distribution plots obtained with the TIE method. After several tests we found that a good compromise both in computational time and in numerical accuracy is to use $N = 3$. In the calculations of the OAM spectrum and thus of the asymmetry parameter q , from the data provided by the EHT, we find the maximum error of q being on the order of 3.4%.

From the values of q and their associated error intervals obtained so far, we then calculate numerically $|\Delta a_{EHT}|$, as reported in Figure 7. To calculate the indetermination in the rotation parameter, we have estimated that the routine used to determine the intensity at the point $P(x, y)$ through the TIE introduces a maximum error due to the variable precision arithmetic method of the numerical routines in Matlab on the order of $\sim 10^{-12}$. The other source of numerical noise is due to the numerical simulations of the Kerr spacetime and Einstein ring that are based on the freely available software package KERTAP (Chen et al. 2015). KERTAP characterizes the propagation of light in Kerr spacetime with very high precision with a deviation on the order of 10^{-7} . This contribution that we call $|\Delta a|_{TIE}$ is almost negligible when compared with the error for a which is introduced by the uncertainties of the asymmetry parameter q , being on the order of $\sim 3.46\%$ and calculated by inserting in the numerical interpolation that relates the two parameters a and q , the values of q in epoch 1 and epoch 2. Applying elementary error theory to the two values of q considered as values of two independent acquisitions with their errorbars, one easily recovers $|\Delta a|_{EHT} = 0.046$.

From the error analysis, the total contribution to the error of a is composed by these two terms, the one introduced by EHT experimental errors in the determination of q and a and those due to the small numerical noise caused by the calculation of the TIE equation and of the OAM spectrum. Summing the two contributions, and being the numerical noise almost negligible, we obtain the total maximum error on the determination of the rotation parameter dominated by the contribution introduced by the experimental data,

$$|\Delta a|_{\text{tot}} = |\Delta a|_{TIE} + |\Delta a|_{EHT} = 0.046 \quad (15)$$

hence yielding a first estimate of the rotation parameter. We found that $a = 0.904 \pm 0.046$, from the averaged asymmetry in the spiral spectrum of $\bar{q} = 1.393 \pm 0.024$ measured in epoch 1 and epoch 2 as described in the main text. We adopt the conservatively approximated value $a = 0.90 \pm 0.10$, as reported in the main text, with an error with 95% confidence interval as shown in Fig. 7.

As reported in Table 1 of the main text, different values of the inclination parameter i yield different families of

asymmetry parameters q that do not overlap, as shown in Fig. 8. In this figure we plot the two curves obtained by the interpolation of the values of a with respect to q for the two values $i = 17^\circ$ and $i = 46^\circ$, with their respective 95% confidence intervals and in the determination of a from q no degeneracy or overlapping between the two curves, is observed. The plot also show the experimental data that fit well with the simulations for the inclination $i = 17^\circ$. We point out that to estimate the rotation parameter a with a single measurement of q if the inclination i is unknown, one has to compare the intensity plots obtained from the observations with the numerical simulations of the BH surroundings, as was done by the EHT team. Another way could be to use a set of different plots of spatial phase distributions that can be obtained during a single observation session by dephasing the receiving antennas and obtain a family of different values of q . This procedure resembles the methods used during the 2011 public experiment of OAM radio transmission and detection in San Marco, Venice, by moving one of the antennas of the interferometer to spatially sample the twisted wave and tune the OAM radio on the twisted channel from the untwisted one (Tamburini et al. 2012). Of course, a better procedure can be made by introducing electronic delays in each of the antennas in the interferometer and/or with a posteriori analysis of the available data.

REFERENCES

- Allen L., Padgett M., 2011, in Torres J. P., Torner L., eds, , Twisted Photons: Applications of Light With Orbital Angular Momentum. Wiley-Vch Verlag, John Wiley and Sons, Weinheim, DE, Chapt. 1, pp 1–12
- Anderson T. W., 1994, Statistical Analysis of Time Series. John Wiley & Sons, New York, NY, USA
- Anzolin G., Tamburini F., Bianchini A., Umbriaco G., Barbieri C., 2008, *Astron. Astrophys.*, 488, 1159
- Bambi C., Freese K., Vagnozzi S., Visinelli L., 2019, preprint (arXiv:1904.12983), p. 8
- Barbero S., 2006, *Opt. Express*, 45, 094001
- Barnett S. M., Allen L., 1994, *Opt. Commun.*, 110, 670
- Beckwith K., Done C., 2005, *Mon. Not. Roy. Astron. Soc.*, 359, 1217
- Cappellari M., et al., 2011, *Monthly Notices of the Royal Astronomical Society*, 413, 813
- Carini P., Geng L.-L., Li M., Ruffini R., 1992, *Phys. Rev. D*, 46, 5407
- Chen B., Kantowski R., Dai X., Baron E., Maddumage P., 2015, *Astrophys. J. Suppl. Ser.*, 218, 4
- Christodoulou D., Ruffini R., 1971, *Phys. Rev. D*, 4, 3552
- Davis L. W., Patsakos G., 1981, *Opt. Lett.*, 6, 22
- De Zela F., 2012, in Pahlavani M. R., ed., , Theoretical Concepts of Quantum Mechanics. IntechOpen, Weinheim, DE, Chapt. 14, pp 289–312
- Dehnen H., 1973, *Int. J. Theor. Phys.*, 7, 467
- Doeleman S. S., Fish V. L., Schenck D. E., et al., 2012, *Science*, 338, 355
- Doi A., Hada K., Nagai H., Kino M., Honma M., Akiyama K., Oyama T., Kono Y., 2013, *EPJ Web of Conferences*, 61, 08008
- EHT Collaboration 2019a, EHT Data Products, Online image data, <https://eventhorizontelescope.org/for-astronomers/data>
- EHT Collaboration 2019b, *Astrophys. J. Lett.*, 875, L1(17)
- EHT Collaboration 2019c, *Astrophys. J. Lett.*, 875, L2(28)
- EHT Collaboration 2019d, *Astrophys. J. Lett.*, 875, L3(32)
- EHT Collaboration 2019e, *Astrophys. J. Lett.*, 875, L4(52)
- EHT Collaboration 2019f, *Astrophys. J. Lett.*, 875, L5(31)
- EHT Collaboration 2019g, *Astrophys. J. Lett.*, 875, L6(44)
- Falcke H., Biermann P. L., 1995, *Astron. Astrophys.*, 293, 665
- Feng L.-L., Lee W., 2001, *Int. J. Mod. Phys. D.*, 10, 961
- Goodman J. W., 1996, Introduction to Fourier Optics, 3 edn. Roberts, Englewood, CO, USA
- Harwit M., 2003, *Astrophys. J.*, 597, 1266
- Kelly D. P., 2018, *Int. J. of Optics*, 2018, 1
- Kerr R. P., 1963, *Phys. Rev. Lett.*, 11, 237
- Lubk A., Guzzinati G., Börrnert F., Verbeeck J., 2013, *Phys. Rev. Lett.*, 111, 173902
- Molina-Terriza G., Torres J. P., Torner L., 2007, *Nature Phys.*, 3, 305
- NED 2019, NED – NASA/IPAC Extragalactic Database. The NASA/IPAC Extragalactic Database (NED) is funded by the National Aeronautics and Space Administration and operated by the California Institute of Technology, <https://ned.ipac.caltech.edu/node/7>
- Ruelas A., Lopez-Aguayo S., Gutiérrez-Vega J. C., 2018, *J. Opt.*, 21, 015602
- Rybicki G. B., Lightman A. P., 2004, Radiative Processes in Astrophysics. Physics Textbook, Wiley, Weinheim
- Schulze C., Naidoo D., Flamm D., Schmidt O. A., Forbes A., Duparré M., 2012, *Opt. Express*, 20, 19714
- Shvedov V., Krolikowski W., Volyar A., Neshev D. N., Desyatnikov A. S., Kivshar Y. S., 2005, *Opt. Express*, 13, 7393
- Sob'yanin D. N., 2018, *Mon. Not. Roy. Astron. Soc. Lett.*, 479, L65
- Su F. S., Mallett R. L., 1980, *Astrophys. J.*, 238, 1111
- Tamburini F., Thidé B., Molina-Terriza G., Anzolin G., 2011a, *Nature Phys.*, 7, 195
- Tamburini F., Mari E., Thidé B., Barbieri C., Romanato F., 2011b, *Appl. Phys. Lett.*, 99, 204102
- Tamburini F., Cuofano C., Valle M. D., Gilmozzi R., 2011c, *Astron. Astrophys.*, 533, A71
- Tamburini F., Mari E., Sponselli A., Thidé B., Bianchini A., Romanato F., 2012, *New J. Phys.*, 14, 03301
- Thidé B., et al., 2007, *Phys. Rev. Lett.*, 99, 087701
- Thidé B., Elias II N. M., Tamburini F., Mohammadi S. M., Mendonça J. T., 2011, in Torres J. P., Torner L., eds, , Twisted Photons: Applications of Light With Orbital Angular Momentum. Wiley-Vch Verlag, John Wiley and Sons, Weinheim, DE, Chapt. 9, pp 155–178
- Thidé B., Tamburini F., Then H., Someda C. G., Ravanelli R. A., 2014, preprint (arXiv:1410.4268), p. 34
- Torner L., Torres J. P., Carrasco S., 2005, *Opt. Express*, 13, 873
- Torres J. P., Torner L., 2011, Twisted Photons: Applications of Light With Orbital Angular Momentum. Wiley-Vch Verlag, John Wiley and Sons, Weinheim, DE
- Wold H., 1954, A Study in the Analysis of Stationary Time Series, 2 edn. Almqvist & Wiksell, Uppsala, Sweden
- Yang H., Casals M., 2014, *Phys. Rev. D*, 90, 023014
- Zhang D., Feng X., Cui K., Liu F., Huang Y., 2015, *Sci. Rep.*, 5, 11982
- van Putten M. H. P. M., 1999, *Science*, 284, 115
- van Putten M. H. P. M., Ostriker E. C., 2001, *The Astrophysical Journal*, 552, L31

This paper has been typeset from a $\text{\TeX}/\text{\LaTeX}$ file prepared by the author.